

## Wave field extrapolation in spatial-domain

***Citation for published version (APA):***

Martens, L. P., Nijmeijer, H., Lopez Arteaga, I., & Moers, E. M. T. (2014). *Wave field extrapolation in spatial-domain*. (D&C; Vol. 2014.006). Eindhoven University of Technology.

***Document status and date:***

Published: 01/01/2014

***Document Version:***

Publisher's PDF, also known as Version of Record (includes final page, issue and volume numbers)

***Please check the document version of this publication:***

- A submitted manuscript is the version of the article upon submission and before peer-review. There can be important differences between the submitted version and the official published version of record. People interested in the research are advised to contact the author for the final version of the publication, or visit the DOI to the publisher's website.
- The final author version and the galley proof are versions of the publication after peer review.
- The final published version features the final layout of the paper including the volume, issue and page numbers.

[Link to publication](#)

***General rights***

Copyright and moral rights for the publications made accessible in the public portal are retained by the authors and/or other copyright owners and it is a condition of accessing publications that users recognise and abide by the legal requirements associated with these rights.

- Users may download and print one copy of any publication from the public portal for the purpose of private study or research.
- You may not further distribute the material or use it for any profit-making activity or commercial gain
- You may freely distribute the URL identifying the publication in the public portal.

If the publication is distributed under the terms of Article 25fa of the Dutch Copyright Act, indicated by the "Taverne" license above, please follow below link for the End User Agreement:

[www.tue.nl/taverne](http://www.tue.nl/taverne)

***Take down policy***

If you believe that this document breaches copyright please contact us at:

[openaccess@tue.nl](mailto:openaccess@tue.nl)

providing details and we will investigate your claim.

# Wave field extrapolation in spatial-domain

L.P. Martens

D&C 2014.006

D&C report

Daily supervisor: Ir. E. Moers  
Supervisor: Prof.dr.ir. I. Lopez-Areaga

Eindhoven University of Technology  
Department of Mechanical Engineering  
Dynamics & Control

Eindhoven, January, 2014

# Contents

<b>1</b>	<b>Introduction</b>	<b>1</b>
<b>2</b>	<b>Theory of wave propagation</b>	<b>2</b>
2.1	Plane waves . . . . .	2
2.2	Acoustic monopole . . . . .	3
2.3	Propagation in wavenumber-domain . . . . .	4
2.3.1	Preconditioning . . . . .	5
2.4	Propagation in spatial-domain . . . . .	6
<b>3</b>	<b>Numerical implementation</b>	<b>10</b>
3.1	Wavenumber-domain . . . . .	10
3.1.1	Preconditioning . . . . .	10
3.1.2	Propagation matrix $\mathbf{E}$ . . . . .	11
3.2	Spatial-domain . . . . .	12
3.2.1	Propagation matrix $\mathbf{W}^+$ . . . . .	13
3.3	Error definition . . . . .	14
<b>4</b>	<b>Numerical simulation</b>	<b>16</b>
4.1	Wavenumber-domain: determine preconditioning parameters . . . . .	16
4.2	Spatial-domain . . . . .	18
4.2.1	Position of the hologram plane . . . . .	18
4.2.2	Position of plane at $z = z_s$ . . . . .	20
4.2.3	Frequency of the source . . . . .	21
4.2.4	Size of the holograms . . . . .	22
4.2.5	Resolution of the wave field . . . . .	26
4.3	Comparison between wave- and spatial-domain propagation . . . . .	27
<b>5</b>	<b>Conclusion</b>	<b>29</b>
<b>A</b>	<b>Normal derivative of <math>G</math></b>	<b>31</b>

# Chapter 1: Introduction

Wave field extrapolation is a technique, which is used for all kinds of applications. It can be used for acoustical modelling in enclosed spaces. To find out how sound waves behave in a certain space. But is also used for source localization. This is often used to find vibrating parts in machines, which produce noise and influence the performance of the machine. When the sources are located it is possible to try to decrease the vibrations. Another application can be found in seismic imaging, where it is used for imaging earth's surface characteristics. The method used in this report for spatial propagation is adopted from this seismic imaging field and is described in Berkhout's paper [2].

In this report a start is made with wave field propagation in wavenumber-domain and in spatial domain. These approaches can then be compared to determine which method gives the most accurate results. The propagation problems for both approaches will be threaded in half space.

First the theory of acoustic waves is briefly discussed. Secondly the theory behind spatial- and wavenumber-domain propagation is studied. After which the numerical implementation of this theory is explained. Then some numerical simulations are performed to improve the implementations and to show their performance. Finally both approaches are compared, for the specific setup that is considered.

# Chapter 2: Theory of wave propagation

In this chapter first the wave theory needed for deriving the theory of wave propagation is discussed. Then the source used for the simulations is explained. And finally the theory of propagation in wavenumber- and spatial-domain is explained.

## 2.1 Plane waves

A wavefield  $p(\vec{r}, t)$  satisfies the acoustic wave equation

$$\nabla^2 p(\vec{r}, t) - \frac{1}{c^2} \frac{\partial^2 p(\vec{r}, t)}{\partial t^2} = 0. \quad (2.1)$$

Here  $\vec{r}$  represents the position in space and  $t$  represents the time. [1] Valid for a homogeneous fluid with no viscosity and if there are no sources in the volume to which it is applied. The speed of sound is represented by  $c$ . When the Fourier transform of the time domain wave equation 2.1 is computed, then this results in

$$\nabla^2 p(\vec{r}, \omega) + k^2 p(\vec{r}, \omega) = 0, \quad (2.2)$$

the Helmholtz equation [1]. This equation can be used to describe harmonic wave propagation. The wavenumber  $k$  is defined as

$$k = \frac{\omega}{c} = \frac{2\pi}{\lambda}. \quad (2.3)$$

The general solution of the Helmholtz equation will be considered here and is shown below

$$p(\omega) = A(\omega) e^{i(k_x x + k_y y + k_z z)}. \quad (2.4)$$

This equation represents a plane wave, which is illustrated in figure 2.1.1.

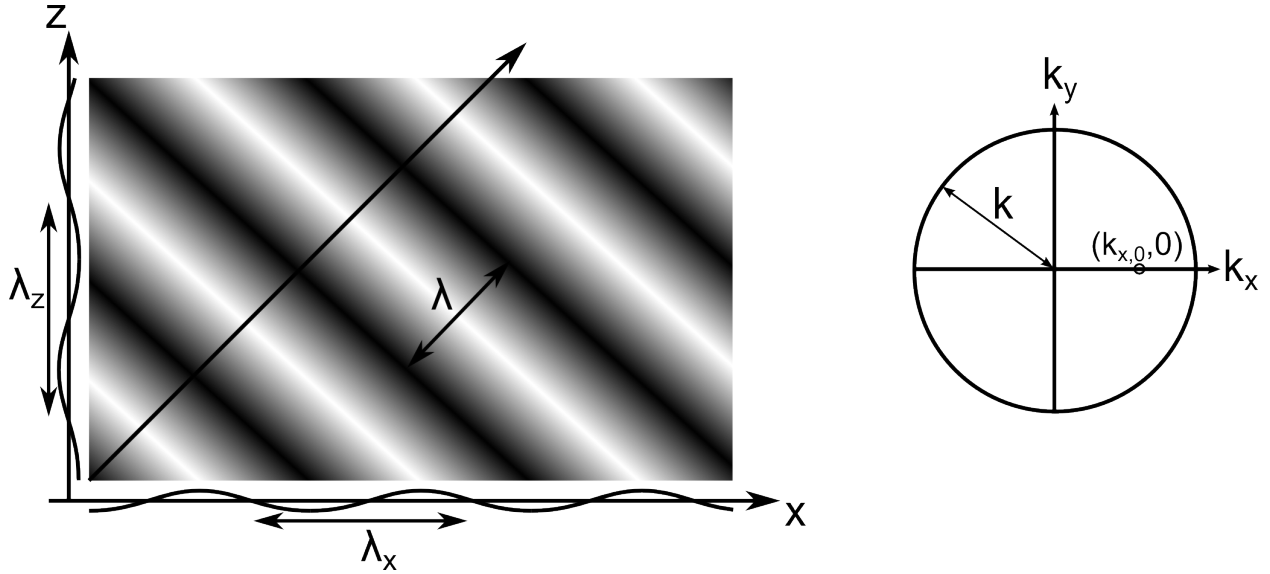


Figure 2.1.1: Illustration of a plane wave

In this equation  $A$  is an arbitrary constant and  $k_x$ ,  $k_y$  and  $k_z$  are the wavenumbers in respectively the  $x$ ,  $y$  and  $z$  direction. Equation 2.4 satisfies the Helmholtz equation when equation 2.5 is met.

$$k^2 = (k_x^2 + k_y^2 + k_z^2) \quad (2.5)$$

Note that equation 2.4 can also be represented as

$$p(\omega) = A(\omega)e^{i(\vec{k} \cdot \vec{r})}. \quad (2.6)$$

Where  $\vec{r} = x\hat{i} + y\hat{j} + z\hat{k}$  represents the position vector and  $\vec{k} = k_x\hat{i} + k_y\hat{j} + k_z\hat{k}$  is representing the direction of the wave propagation.

## 2.2 Acoustic monopole

In this report only a monopole source is used. A plane wave (equation 2.6) propagates in one direction, so the wave direction  $\vec{k}$  and the pressure field  $|p(\omega)|$  are constant for every position  $\vec{r} = (x, y, z)$ . Sound waves from a monopole source propagate in every direction. When the origin of  $\vec{r}$  is located at the position of the source, then the wave direction  $\vec{k}$  is always equal to the direction of the vector  $\vec{r}$ . And now the amplitude of the pressure field  $|p(\omega)|$  is only dependent on the distance of the source  $|\vec{r}|$ . The monopole source is described with

$$p(\omega) = \frac{A(\omega)}{|\vec{r}|} e^{i(|\vec{k}| \cdot |\vec{r}|)} \quad (2.7)$$

and visualised in figure 2.2.1.

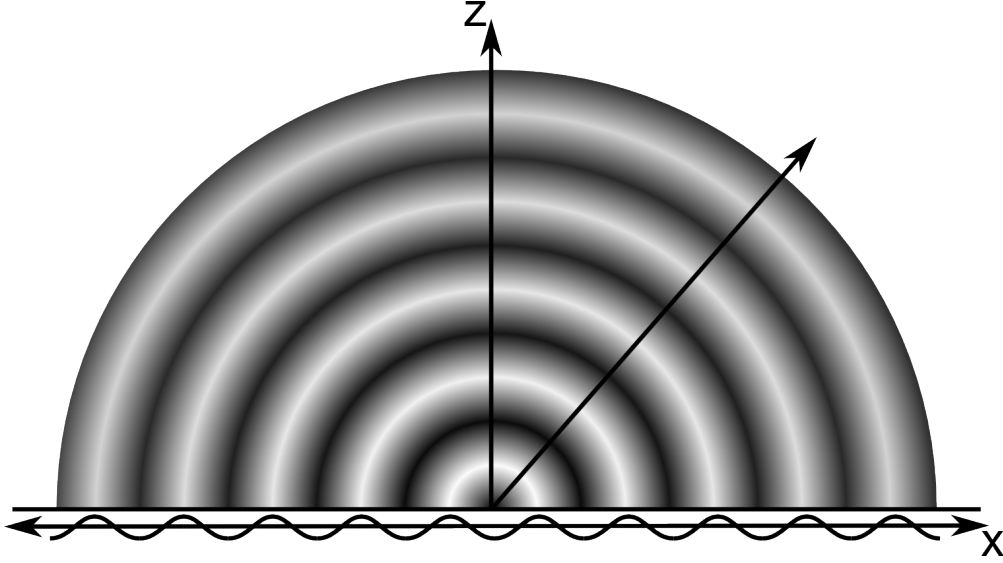


Figure 2.2.1: Visualisation of the acoustic monopole

## 2.3 Propagation in wavenumber-domain

Since  $k$  is defined as equation 2.3, in which  $\omega$  is the frequency and  $c$  is the speed of sound, the wavenumber  $k$  is constant. This means that the three directional wavenumbers are dependent on each other. Maximum two variables are independent, therefore one variable can be chosen dependent. Regarding the wavenumber domain in this document  $k_z$  is chosen as dependent variable, as

$$k_z^2 = k^2 - k_x^2 - k_y^2. \quad (2.8)$$

Now a steady state wave field  $p(x, y, z, \omega)$  is considered. This pressure field is a summation of the plane waves present in the source-free half space. This summation is represented as

$$p(x, y, z, \omega) = \sum_{k_x} \sum_{k_y} P(k_x, k_y) e^{i(k_x x + k_y y + k_z z)} \quad (2.9)$$

in which the exponential term can be recognized as a plane wave. When this pressure field is considered at position  $z = 0$ , equation 2.10 is obtained;

$$P(k_x, k_y, 0) = \mathcal{F}_x \mathcal{F}_y [p(x, y, 0, \omega)] \quad (2.10)$$

this equation describes the Fourier transformation in  $x$  and  $y$  direction of the wave field, and results in the wave field representation in wavenumber domain. The wave field description in wavenumber domain is now used to do the propagation to another plane. This is possible

because of the relation between  $z = 0$  and  $z = \text{constant}$ . This results in the general expression

$$P(k_x, k_y, z) = P(k_x, k_y, z')e^{i(k_z z - z')} \quad (2.11)$$

used for forward propagation in wavenumber domain from plane  $z = z'$  to plane  $z = z$ . Equation 2.11 shows that the wave amplitudes only undergo a phase change, when  $k_z$  is real. These are propagating waves. When  $k_z$  are imaginary the waves die out. After this propagation the inverse Fourier transformation is needed to obtain the propagated wave field  $p(x, y, z, \omega)$ .

### 2.3.1 Preconditioning

Because of the discrete Fourier transformation, which has to be applied to the wave field, this implements some errors to the results in wavenumber domain. Those problems are due to the fact that the wave field is only known at specific discrete points and because the aperture is finite.

Because the aperture is finite, nothing is known of the wave field outside of the plane borders. When a fft is performed on this finite aperture, then this is equivalent to performing the fft on an infinite signal created by replicating the measured aperture. This will result in a wave field, which will most likely contain discontinuities at the position where the repetitive planes are attached to each other, shown in figure 2.3.1.

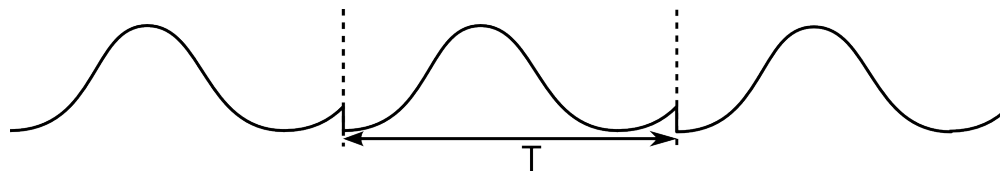


Figure 2.3.1: Development of discontinuities

Those sharp discontinuities will result in a large frequency domain needed, to be able to describe the wave field, using the fft. Therefore when a fft is applied to a sine wave of a certain frequency, this should result in a single frequency line. But because of the finite data this single frequency line will be spread out and form a wide peak. This issue is called spectral leakage [5]. To reduce the effects of spectral leakage the discontinuities should be reduced. This can be done by applying a window to the wave field. This window should be some sort of function which smoothly reduces the wave field to zero at the plane border. The window which will be used is specified in chapter 3.1.

A disadvantage of using a window function on the wave field is that a lot of information of the wave field is lost. This loss of information can result in large errors when the wave field in wavenumber space is propagated. A window with steep sides does not alter the information, but it also gives a less smooth transition to zero at the border. This results in errors due to the increase of spectral leakage. To retain as much information as possible and reduce



spectral leakage, border padding is applied: the plane will be enlarged using the data values of the wave field at the border of the plane, which is shown for 1 dimensions in figure 2.3.2.

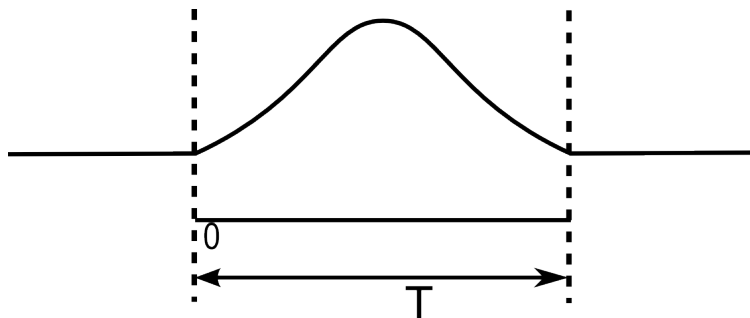


Figure 2.3.2: Border padding

After border padding, the window is applied. The addition of border padding results in less information loss of the original wave field. In figure 2.3.3 the idea of border padding is shown. In this figure it is also visible that the use of border padding also introduces a discontinuity, of which the effect is further discussed in 3.1.

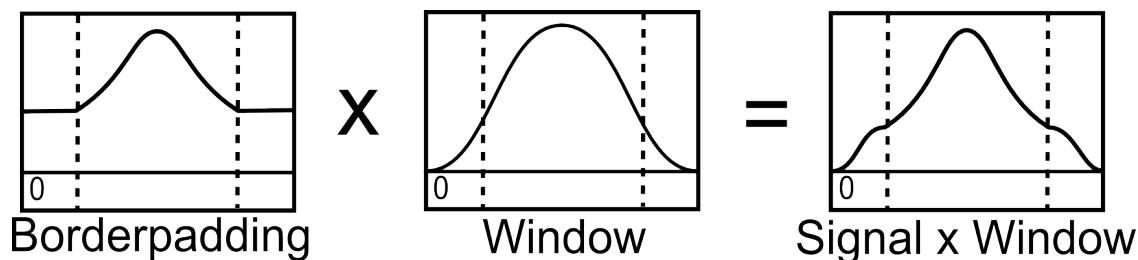


Figure 2.3.3: Border padding

## 2.4 Propagation in spatial-domain

Huygen's principle states that the propagation of a wave through a certain medium can be described by adding the contributing of all secondary sources, positioned along a wave front. Which means that the wave field inside a source free volume can be described using secondary sources positioned at the boundary surface. These secondary sources are created at the boundary surface as a result of the primary sources surrounding this boundary. This property can be described by the Kirchhoff integral [2]:

$$P_A = \frac{1}{4\pi} \oint_S \left[ \frac{e^{-jkr}}{r} \rho_0 j \omega V_n + P \frac{1 + jkr}{r^2} e^{-jkr} \cos \varphi \right] \hat{n} dS \quad (2.12)$$

The Kirchhoff integral comes from the substitution of the wave equation in Green's second theorem;

$$\oint_V [F\nabla^2 G - G\nabla^2 F]dV = \oint_S [P\nabla G - G\nabla P]\hat{n}dS. \quad (2.13)$$

A closed surface of which the volume it encloses is source free is assumed.  $F$  is chosen as the pressure field generated by the sources outside of the source free volume . So  $F$  is defined as:

$$F = P(x, y, z, \omega). \quad (2.14)$$

$P$  satisfies the Helmholtz equation 2.2. Now it is supposed that the Green function satisfies

$$G = \frac{e^{-jkr}}{r}, \quad (2.15)$$

the Green's function for infinite space [4] with

$$|\vec{r}| = \sqrt{(x - x_0)^2 + (y - y_0)^2 + (z - z_0)^2}. \quad (2.16)$$

Because  $G$  satisfies

$$\nabla^2 G + k^2 G = -4\pi\delta(x - x_\alpha)\delta(y - y_\alpha)\delta(z - z_\alpha), \quad (2.17)$$

this will make Green's theorem, using the shift theorem, become equal to

$$\oint_S [P\nabla G - G\nabla P]\hat{n}dS = -4\pi P_A \quad (2.18)$$

according to paper [3]. In which  $P_A$  represents the pressure at a position  $A$  in the source free volume.

The normal derivatives of  $G$  and  $P$  in this equation have to be determined. The pressure gradient is related to the velocity as;

$$\nabla P = -\rho_0 \frac{\partial V}{\partial t}. \quad (2.19)$$

So for the normal derivative

$$\frac{\partial P}{\partial \vec{n}} = -\rho_0 \frac{\partial V}{\partial t} \quad (2.20)$$

is obtained. When is considered that  $V(x, y, z, t) = f(x, y, z)\exp(-j\omega t)$  then the normal derivation of the pressure is computed as

$$\frac{\partial P}{\partial \vec{n}} = \rho_0 j\omega V_n. \quad (2.21)$$

When the normal direction is defined in the positive  $z$  direction , the normal derivation of the Green's function becomes

$$\frac{\partial G}{\partial \vec{n}} = \frac{\partial G}{\partial r} \frac{\partial r}{\partial z}. \quad (2.22)$$

The normal derivative of  $G$  can now be determined. Which leads to

$$\frac{\partial G}{\partial n} = -\frac{1 + jkr}{r^2} e^{-jkr} \cos \varphi, \quad (2.23)$$

the complete derivation is described in appendix A. The rearrangement of equation 2.18 leads to

$$P_A = \frac{1}{4\pi} \oint_S [G \nabla P - P \nabla G] \hat{n} dS \quad (2.24)$$

and the substitution of  $\frac{\partial P}{\partial n}$ ,  $G$  and  $\frac{\partial G}{\partial n}$  in equation 2.24 will then result in

$$P_A = \frac{1}{4\pi} \oint_S \left[ \frac{e^{-jkr}}{r} \rho_0 j \omega V_n + P \frac{1 + jkr}{r^2} e^{-jkr} \cos \varphi \right] \hat{n} dS. \quad (2.25)$$

So equation 2.25 results in the Kirchhoff-Helmholtz integral, formulated in the space-frequency domain, used in paper [2]. A representation of this integral is given in figure 2.4.1.

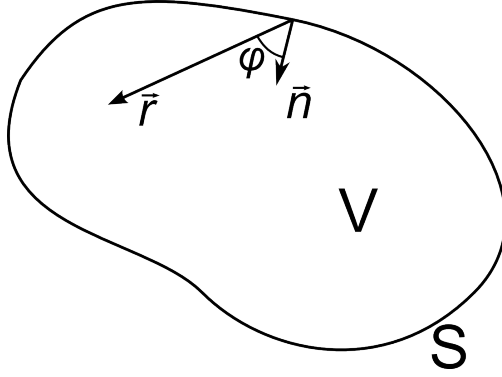


Figure 2.4.1: Visualisation of the Kirchhoff-Helmholtz integral

Using this equation the pressure can be calculated at any point inside of the surface  $S$ , when all secondary sources are known. But because planar propagation is desired the Green's function  $G$  needs to be replaced by

$$G = \frac{e^{-jkr}}{r} - \frac{e^{-jkr'}}{r'} \quad (2.26)$$

Which is the Green's function that applies to plane screens. In this function  $r' = r$ . The normal derivation of  $r$  is now  $\delta r / \delta n = -\delta r' / \delta n$ . Therefore the normal derivation of the Green's function will now be equal to

$$\frac{\partial G}{\partial n} = -2 \frac{1 + jkr}{r^2} e^{-jkr} \cos \varphi. \quad (2.27)$$

Using Green's function 2.26, equation 2.24 will result in a degenerated form of a closed surface integral

$$P(r_1, \omega) = \frac{1}{2\pi} \int_{-\infty}^{\infty} \int_{-\infty}^{\infty} [P(r_0, \omega) \frac{1 + jkr}{r^2} e^{-jkr} \cos \varphi] dx dy. \quad (2.28)$$

This equation represents an infinite plate surface between the source and the receiver domain, which is known as the Rayleigh II integral in three-dimensions, which forms the basis of the wave-field extrapolation in spatial domain.  $r_1$  and  $r_0$  are related to the planes  $z_1$  and  $z_0$  respectively. The general representation of the Rayleigh II integral is

$$P(x_1, y_1, z_1, \omega) = \int_{-\infty}^{\infty} \int_{-\infty}^{\infty} [W(x_1 - x, y_1 - y, z_1 - z, \omega) P(x_0, y_0, z_0, \omega)] dx dy \quad (2.29)$$

of which a visualisation is shown in figure 2.4.2, where

$$W(x_1 - x, y_1 - y, z_1 - z, \omega) = \frac{\cos \varphi}{2\pi} \frac{1 + jkr}{r^2} e^{-jkr} \quad (2.30)$$

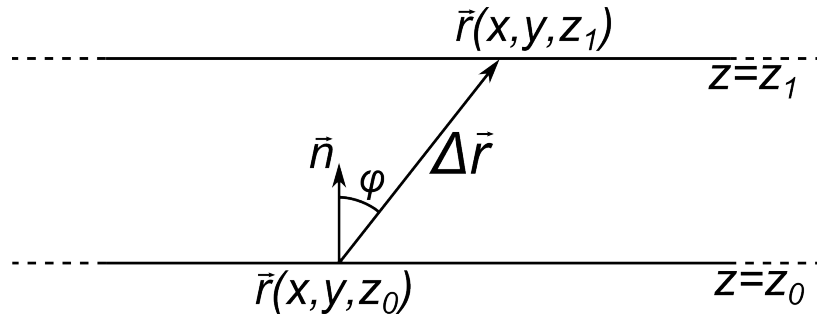


Figure 2.4.2: Visualisation of the RayleighII integral

In acoustic holography only discrete points of a finite pressure field are known, therefore equation 2.28 is replaced by

$$P^+(z_1) = \mathbf{W}^+ P^+(z_0) \quad (2.31)$$

This equation consists of  $P^+(z_1)$ , the unknown discrete pressure field in the receiver domain at position  $z_1$ ,  $P^+(z_0)$ , the known discrete pressure field at position  $(z_0)$  and  $\mathbf{W}^+$  the propagation matrix containing all extrapolation components for all relevant combinations of  $r_0$  and  $r_1$ . The exact realization of this propagation equation is explained in section 3.2.

# Chapter 3: Numerical implementation

In this chapter the numerical implementations of the propagation theory are discussed. At first the wavenumber-domain is discussed and secondly the spatial-domain is discussed. Finally the error calculation is defined.

Both numerical implementations first determine the wave fields at the plane at  $z = z_s$  and at  $z = z_h$  directly using the monopole equation 2.7. After this compilation both implementations propagate the wave field from the plane at  $z = z_s$  to the plane at  $z = z_h$ . After which the difference, between the direct calculated pressure field  $z_h$  and the pressure field propagated from  $z_s$  by both methods, is determined. The simulation configuration is shown in figure 3.0.1.

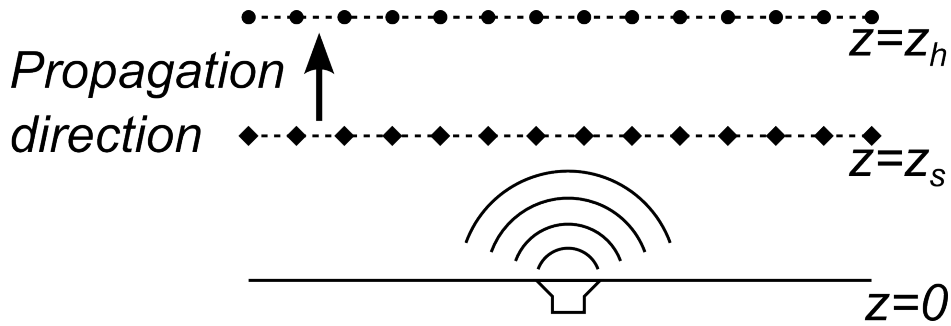


Figure 3.0.1: Free-field configuration

## 3.1 Wavenumber-domain

The entire computation in wavenumber-domain is represented in figure 3.1.1.

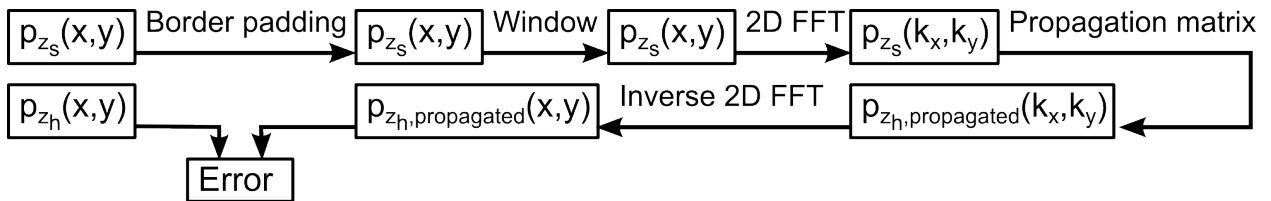


Figure 3.1.1: Wavenumber-domain computation

Before applying the 2 dimensional fft to the pressure field  $p_{z_s}$  preconditioning is utilized. Then the wave field  $P_{z_s}(k_x, k_y)$  can be multiplied by the propagation matrix, which results in the wave field  $P_{z_h,propagated}(k_x, k_y)$ . After the inverse 2 dimensional fft, the wave field in frequency domain  $p_{z_s,propagated}$  is achieved.

### 3.1.1 Preconditioning

At first border padding is used. This will increase the size of the aperture using the data values of the border of the wave field  $p_{z_s}$ . The amount of surface that is added to the

border of the wave field can be varied, which will influence the error of the final wave field  $p_{z_s, propagated}$ . Now a window is applied to the border padded plane. The Tukey window which is used consists of three sections: taper, constant and taper. The tapers are defined as the halves of a cosine and the parameter determines the fraction, between 0 and  $\pm 0.5$ , which is used for these halve cosines. The space between the cosines is kept constant at the value 1. The Tukey window is shown in figure 3.1.2. The windows vary from a rectangular window (parameter = 0) to a Von Hann window (parameter = 1).

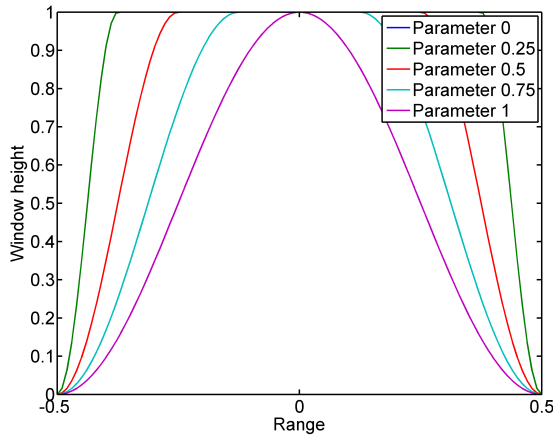


Figure 3.1.2: Windows used to reduce spectral leakage

### 3.1.2 Propagation matrix $\mathbf{E}$

The propagation is based on equation 2.11, which represents the wave propagation of a point  $(k_x, k_y)$  at plane  $z = z_0$  to the same point  $(k_x, k_y)$  at another plane at  $z = z_1$ . Because a whole plane needs to be propagated, equation 2.11 will now be written in matrix form which results in;

$$\mathbf{P}(k_x, k_y, z_1) = \mathbf{P}(k_x, k_y, z_0) \circ \mathbf{E} \quad (3.1)$$

This represents an element by element matrix multiplication, where  $\mathbf{E}$  is the propagation matrix. This means that these matrices are exactly the same size so an element wise multiplication is possible. The exact definition used in the implementation is shown below.

$$\mathbf{P}(z_0) = \begin{pmatrix} p(k_{x,1}, k_{y,1}, z_0) & \cdots & p(k_{x,N}, k_{y,1}, z_0) \\ \vdots & & \vdots \\ p(k_{x,1}, k_{y,M}, z_0) & \cdots & p(k_{x,N}, k_{y,M}, z_0) \end{pmatrix} \quad (3.2)$$

$$\mathbf{P}(z) = \begin{pmatrix} p(k_{x,1}, k_{y,1}, z) & \cdots & p(k_{x,N}, k_{y,1}, z) \\ \vdots & & \vdots \\ p(k_{x,1}, k_{y,M}, z) & \cdots & p(k_{x,N}, k_{y,M}, z) \end{pmatrix} \quad (3.3)$$

Every element of the propagation matrix can now be calculated using

$$E(p(k_x, k_y, (z_1 - z_0))) = e^{ik_z(z_1 - z_0)}, \quad (3.4)$$

where

$$k_z = \sqrt{k^2 - k_x^2 - k_y^2}. \quad (3.5)$$

## 3.2 Spatial-domain

The complete computation in spatial domain is visualised in figure 3.2.1.

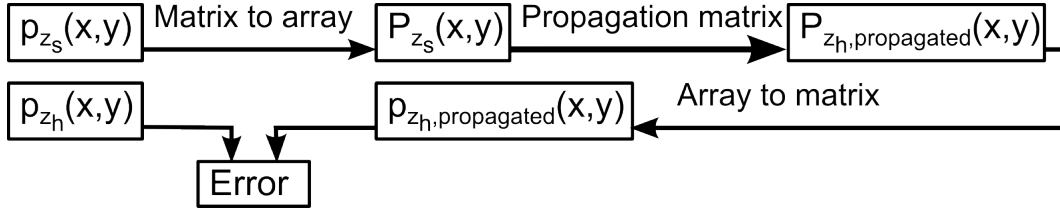


Figure 3.2.1: Spatial-domain computation

The propagation is computed using equation 2.31. This equation consists of two arrays  $\vec{P}^+(z_0)$  and  $\vec{P}^+(z_1)$ .  $\vec{P}^+(z_0)$  contains the pressure at every discrete position of  $p_{z_s}$  and  $\vec{P}^+(z_1)$  contains (after the computation) the pressure at every discrete position of  $p_{z_h,propagated}$ . So when the wave field matrices are of size  $N \times M$  then the wave field arrays are of size  $1 \times R = 1 \times (N \times M)$ . Equation 2.31 also contains the propagation matrix  $\mathbf{W}^+$ , which consists of all propagation components for all combinations of the discrete positions of  $p_{z_s}$  and  $p_{z_h,propagated}$ . Consequently the size of the propagation matrix is equal to  $R \times R$ . The exact definition of these pressure matrices and the propagation matrix are shown below.

$$P^+(z_0) = \begin{pmatrix} p_{z_s,1}(x_1, y_1, z_0) \\ p_{z_s,2}(x_2, y_1, z_0) \\ \vdots \\ p_{z_s,k}(x_j, y_i, z_0) \\ \vdots \\ p_{z_s,R-1}(x_{j-1}, y_M, z_0) \\ p_{z_s,R}(x_N, y_M, z_0) \end{pmatrix} \quad (3.6) \quad P^+(z_1) = \begin{pmatrix} p_{z_h,1}(x_1, y_1, z_1) \\ p_{z_h,2}(x_2, y_1, z_1) \\ \vdots \\ p_{z_h,m}(x_i, y_j, z_1) \\ \vdots \\ p_{z_h,R-1}(x_{j-1}, y_M, z_1) \\ p_{z_h,R}(x_N, y_M, z_1) \end{pmatrix} \quad (3.7)$$

$$\mathbf{W}^+ = \begin{pmatrix} W(p_{z_h,1}, p_{z_s,1}) & \cdots & W(p_{z_h,1}, p_{z_s,k}) & \cdots & W(p_{z_h,1}, p_{z_s,R}) \\ \vdots & & \vdots & & \vdots \\ W(p_{z_h,m}, p_{z_s,1}) & \cdots & W(p_{z_h,m}, p_{z_s,k}) & \cdots & W(p_{z_h,m}, p_{z_s,R}) \\ \vdots & & \vdots & & \vdots \\ W(p_{z_h,R}, p_{z_s,1}) & \cdots & W(p_{z_h,R}, p_{z_s,k}) & \cdots & W(p_{z_h,R}, p_{z_s,R}) \end{pmatrix} \quad (3.8)$$

### 3.2.1 Propagation matrix $\mathbf{W}^+$

Now the computation method to calculate a single component of the propagation matrix needs to be determined.

#### Method 1

The first method that will be used is shown below;

$$W(r_1, r_0) = W(x_1 - x_0, y_1 - y_0, z_1 - z_0, \omega) \Delta x \Delta y, \quad (3.9)$$

where

$$W(x_1 - x_0, y_1 - y_0, z_1 - z_0, \omega) = \frac{\cos \varphi}{2\pi} \frac{1 + jkr}{r^2} e^{-jkr}. \quad (3.10)$$

In this equation  $\Delta x$  and  $\Delta y$  are equal to the distance between two neighbouring positions. This method can be compared to a Riemann sum, of which the accuracy of the approximation is dependent on the resolution of the volume above the surfaces of size  $A = \Delta x \times \Delta y$ .

#### Method 2

The second method used for the calculation of a propagation matrix component is

$$W(r_1, r_0) = \int_{x_0 - \Delta x/2}^{x_0 + \Delta x/2} \int_{y_0 - \Delta y/2}^{y_0 + \Delta y/2} W(x_1 - x_0, y_1 - y_0, z_1 - z_0, \omega) \, dx dy. \quad (3.11)$$



This method gives a better approximation of the volume above the surfaces  $A = \Delta x \times \Delta y$ . A better result is expected when using this method, but this method takes much longer to compute than method 1. Every point of the plane  $p_{z_s}$  is used to calculate one pressure point of the plane  $p_{z_h,propagated}$ . So in the propagation matrix  $\mathbf{W}^+$  every row is needed to calculate one pressure point of plane  $p_{z_h,propagated}$ .

Therefore a lot of calculations are needed to calculate every component, especially when the resolution is increased, which leads rapidly to a very large propagation matrix. But the whole matrix consists of repeating elements. The propagation matrix consists namely out of  $M$  different toeplitz matrices which are themselves arranged in toeplitz order as;

$$\mathbf{W}_{order}^+ = \begin{bmatrix} a & b & c & | & e & f & g & | & i & j & k \\ b & a & b & | & f & e & f & | & j & i & j \\ c & b & a & | & g & f & e & | & k & j & i \\ e & f & g & | & a & b & c & | & a & b & c \\ f & e & f & | & b & a & b & | & b & a & b \\ g & f & e & | & c & b & a & | & c & b & a \\ i & j & k & | & e & f & g & | & a & b & c \\ j & i & j & | & f & e & f & | & b & a & b \\ k & j & i & | & g & f & e & | & c & b & a \end{bmatrix} \quad (3.12)$$

This repetition pattern is used to speed up calculation. Only the components of the first row of the matrix are calculated and all the other rows are built using the components of the first row.

### 3.3 Error definition

The difference between the plane  $p_{z_h}$  and the plane  $p_{z_h,propagated}$  can now be determined. Three errors are used for this evaluation.

First the error if a single point in the middle of the plane is considered. The error of the amplitude and the error of the phase are calculated. The relative error of the amplitude is defined as

$$\epsilon_{amplitude} = \frac{|p_{z_h,prop}| - |p_{z_h}|}{|p_{z_h}|} \cdot 100\%. \quad (3.13)$$

The definition of the relative phase error is a bit more complicated, because the phase is only defined from  $-\pi$  to  $\pi$ . Only the phase difference will be considered, therefore the error is defined as

$$\epsilon_{phase} = \begin{cases} \frac{|arg(p_{z_h}) - 2\pi - arg(p_{z_h,prop})|}{\pi} \cdot 100\% & \text{if } arg(p_{z_h}) \geq 0 \wedge arg(p_{z_h,prop}) < arg(p_{z_h}) - \pi \\ \frac{|arg(p_{z_h,prop}) - arg(p_{z_h})|}{\pi} \cdot 100\% & \text{if } arg(p_{z_h}) \geq 0 \wedge arg(p_{z_h,prop}) \geq arg(p_{z_h}) - \pi \\ \frac{|arg(p_{z_h}) + 2\pi - arg(p_{z_h,prop})|}{\pi} \cdot 100\% & \text{if } arg(p_{z_h}) < 0 \wedge arg(p_{z_h,prop}) > arg(p_{z_h}) + \pi \\ \frac{|arg(p_{z_h,prop}) - arg(p_{z_h})|}{\pi} \cdot 100\% & \text{if } arg(p_{z_h}) < 0 \wedge arg(p_{z_h,prop}) \leq arg(p_{z_h}) + \pi \end{cases} \quad (3.14)$$

The last error considered is the error over the entire plane;

$$\epsilon_{RMS} = \sqrt{\sum_{j=1}^M \sum_{i=1}^N \frac{|p_{z_h}(i, j) - p_{z_h,prop}(i, j)|^2}{|p_{z_h}|^2}} \frac{1}{R} \cdot 100\%. \quad (3.15)$$

So the root of the mean of the squared error is calculated.

# Chapter 4: Numerical simulation

The completed implementations can now be subjected to some simulations, by which the correctness of the implementation for different parameters can be checked. In these tests the parameters  $z_s$ ,  $z_h$ ,  $f$ ,  $\Delta x$ ,  $\Delta y$  and the size of  $z_s$  and  $z_h$  will be kept constant when not stated differently. The values of these parameters are stated below.

- $z_s = 0.1m$
- $z_h = 0.2m$
- $f = 100Hz$
- $\Delta x = 0.1m$
- $\Delta y = 0.1m$
- Aperture size at  $z = z_s$ :  $L_x = L_y = 4.0m$
- Aperture size at  $z = z_h$ :  $L_x = L_y = 4.0m$

## 4.1 Wavenumber-domain: determine preconditioning parameters

The simulations performed in wave-domain are used to determine optimal parameter values. In this case, because the wavenumber-domain will also be compared with the spatial-domain, it is chosen to optimize the parameter values for a range of the position of plane at  $z = z_h$ . The enlargement of the plane, using border padding, is varied for the parameter  $B$ , which determines how much the length of both sides of the aperture is increased. side of the plane is increased. The range of the parameter is;

$$B = [1, 2, 3, 4, 5, 6]. \quad (4.1)$$

The other parameter which is varied is the steepness of the Tukey window, see section 3.1. The variation range of this parameter is;

$$\textit{Steepness - parameter} = [0.1, 0.2, 0.3, 0.4, 0.5, 0.6, 0.7, 0.8, 0.9, 1.0]. \quad (4.2)$$

Finally also the position of the plane at  $z = z_h$  is varied, namely for

$$z_h = [0.2, 1.0, 10]. \quad (4.3)$$

This is done to assure that the parameters can be chosen such that always a reasonable result is obtained, or to see that this is impossible to obtain. The results of changing the border padding size and the slope of the window are shown in figure 4.1.1 for  $z_h = 0.2m$ , in figure 4.1.2 for  $z_h = 1.0m$  and in figure 4.1.3 for  $z_h = 10m$ .

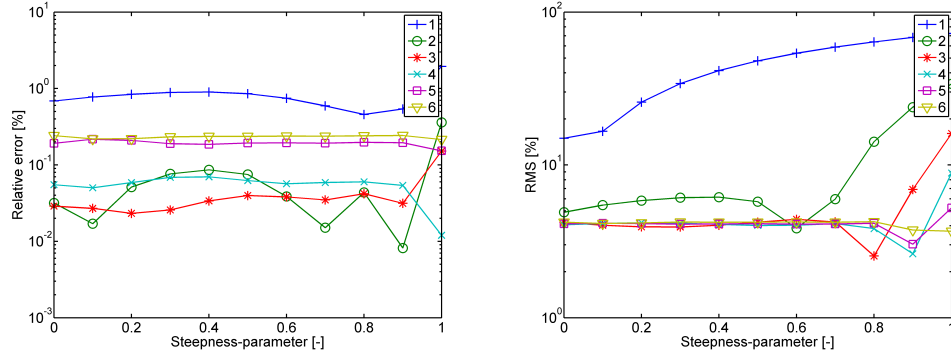


Figure 4.1.1: Relative error versus window steepness-parameter for varying the border padding width at  $z_h = 0.2m$

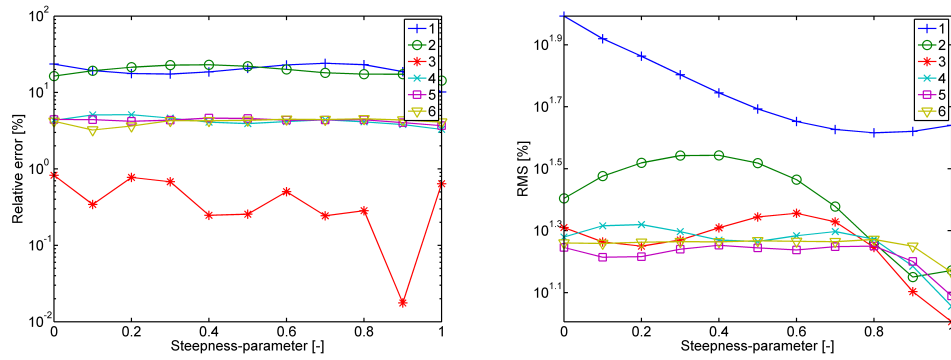


Figure 4.1.2: Relative error versus window steepness-parameter for varying the border padding width at  $z_h = 1.0m$

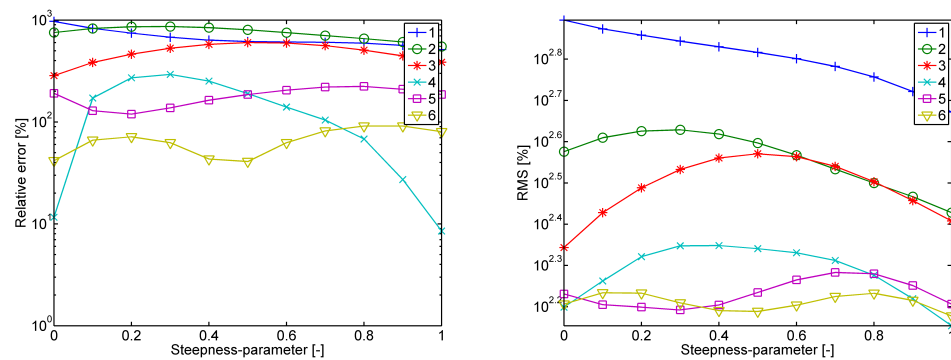


Figure 4.1.3: Relative error versus window steepness-parameter for varying the border padding width at  $z_h = 10m$

Now the average of these errors is determined and the results are shown in figure 4.1.4. These graphs show that 3 times increasing the aperture gives the best result, but this is probably due to the fact that at  $z_h = 1.0m$  the error is really small. Because the error at  $z_h = 1.0m$  is very different compared to the other errors, it might be a coincidence that the error is this small. Therefore this parameter of value 3 is not taken into account. Now 4 times increasing the aperture gives the best result. The steepness parameter is chosen at 0.95, because this gives for all positions of the plane at  $z_h$  a reasonable result. Therefore these parameters will be used when the implementation of wave- and spatial-domain are compared in section 4.3. For spatial domain no preconditioning is used.

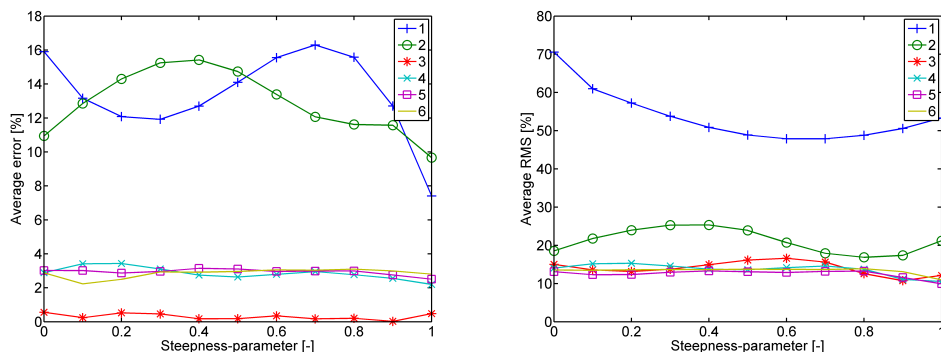


Figure 4.1.4: Average relative error versus window steepness-parameter for varying the border padding width at  $z_h = 0.2m$ ,  $z_h = 1.0m$  and  $z_h = 10m$

## 4.2 Spatial-domain

First simulations are done in spatial-domain to validate the implementation and determine the differences in performance between method 1 and method 2 described in chapter 3.2.

### 4.2.1 Position of the hologram plane

The height of the hologram plane, the plane at  $z = z_h$ , is varied, which will show the difference between near-field and far-field propagation in spatial domain. The simulation setting is shown in figure 4.2.1.

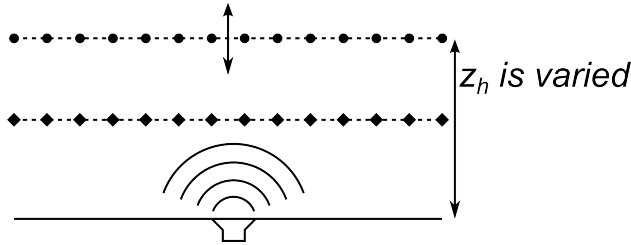


Figure 4.2.1: Simulation setting: varying  $z_h$

In this setting two contrasting cases can occur. First increasing the height  $z_h$  will result in a less detailed hologram, because the wave field produced by the monopole will tend towards a plain wave at infinity. This means that the propagation is easier, because less detail is needed. However the propagation is also made more difficult when increasing the height, because a single wave field is extrapolated to a plane which is located much further away. So it is not clear which case will get the upper hand until the simulations are performed.

The results are shown in figure 4.2.2. These figures show a general trend of an error which increases when the distance from the source  $z_h$  increases. When the distance from the source increases more than  $z_h = 10m$  all errors will tend to a constant value. The figures also show that method 1 gives much worse results below  $z_h = 0.2m$ . This can be explained by the fact that method 1 doesn't provide a good approximation, when the distance between the discrete points becomes much larger than the distance between the planes. But than when looking at the relative and the RMS error it shows that between  $z_h = 0.2m$  and  $z_h = 10m$  method 1 gives a more accurate than method 2. The difference between the two methods is however smaller than one percent and is therefore considered negligible. Also a flaw can be spotted in the relative error between  $z_h = 3m$  and  $z_h = 7m$  where both methods show a large dip in the graph. Some small effects of this can also be seen in the RMS error at  $z_h = 3m$ . But the exact cause of this flaw is yet to be determined.

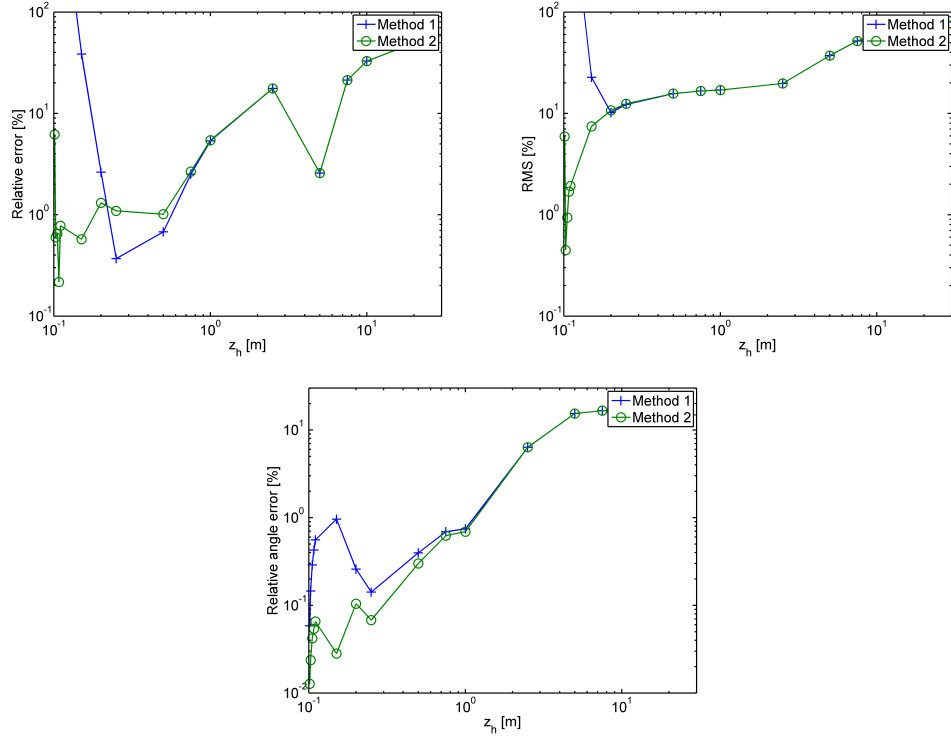


Figure 4.2.2: Errors versus the height  $z_h$  of the hologram plane

#### 4.2.2 Position of plane at $z = z_s$

Now not only the hologram plane is moved but also plane at  $z = z_s$ , while the distance between these two planes will be kept constant. This will lead to two holograms which become less detailed when the height is increased. But the extrapolation distance is kept the same. Therefore a lower error is expected, than in the previous simulation. The simulation setting is visualised in figure 4.2.3.

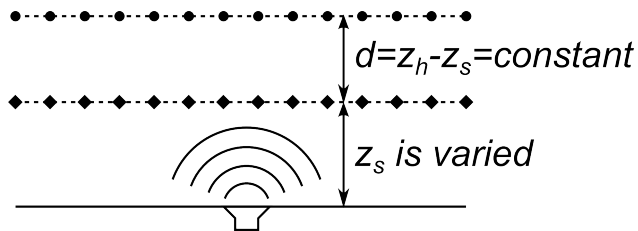


Figure 4.2.3: Simulation setting: varying  $z_s$

The results are shown in figure 4.2.4, in which the distance between the planes is equal to  $d = 0.1m$ . The most striking in these graphs is that below  $z_s = 0.1m$  the error increases

rapidly. This is due to the fact that the hologram is very detailed at this moment because it is so close to the source. This detailed wave field seems to be very difficult to propagate even over a short distance. Another conspicuous point in the relative error is shown between  $z_s = 0.8m$  and  $z_s = 6m$ , where method 1 gives a better result than method 2. But also here the error is less than one percent and is therefore neglected. An more conspicuous point is the fact that method 1 gives a better result than method 2 in the RMS error for the entire range of  $z_s$ . But again the difference between the two methods is less than one percent. Moreover the situation of the RMS error seems to be predictable, because some extra simulations showed that it can be related to the previous simulation (varying the position of the hologram plane). When a position  $z_h$  is chosen in the previous simulation, and the difference between the RMS error of method 1 and method 2 is checked at a certain distance between the planes, it appears that when keeping that same distance will doing this simulation that the difference between the RMS errors remains roughly at the same level.

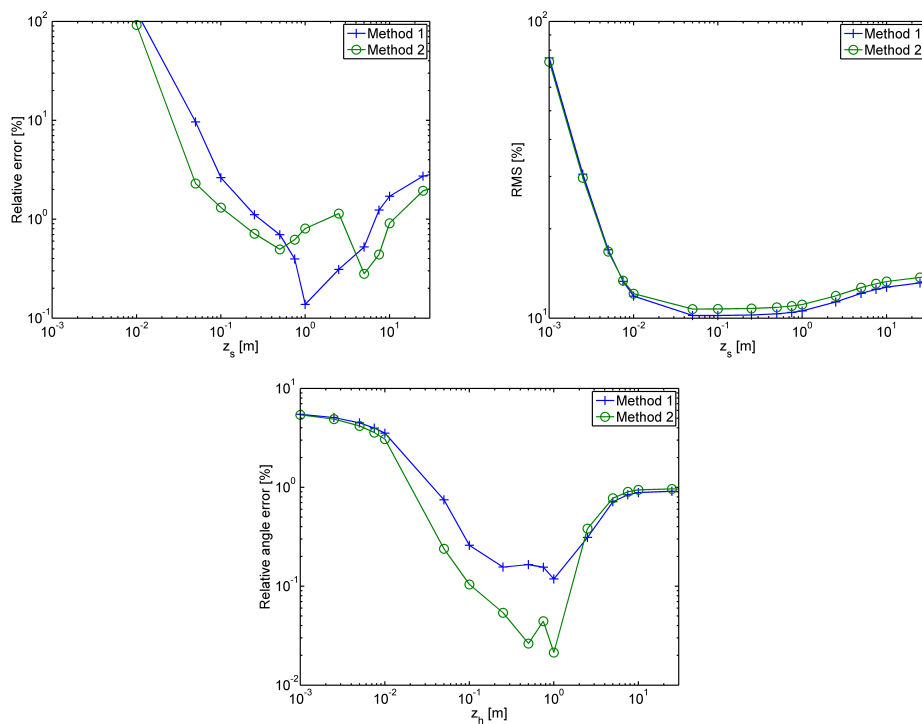


Figure 4.2.4: Errors versus the height of the plane at  $z_s$ , while the distance between the holograms is kept constant

### 4.2.3 Frequency of the source

Here the influence of different source frequencies is considered. Increasing the frequency also increases the wavelength of the source, while decreasing the frequency does exactly the



opposite. A shorter wavelength will result in a more detailed wave field, which might cause problems when applying the propagation.

The simulation results are shown in figure 4.2.5. In every graph can be seen that the accuracy of the propagation is gone when the frequency becomes higher than  $f = 1000\text{Hz}$ . This can be acknowledged because the wavelength at this frequency is equal to  $\lambda = 0.343\text{m}$ , while the resolution is equal to  $res. = 0.1\text{m}$ . And therefore an accurate representation of the wave field is impossible. At the lower frequencies the error seems to remain approximately equal. The relative angle error seems to have some trouble to be calculated correctly when the frequency is increased. This can make sense, because the phase changes much faster at higher frequencies. The only inexplicable error is found in the relative error at  $f = 600\text{Hz}$ , where the error of method 1 is quite small, while method 2 is not effected.

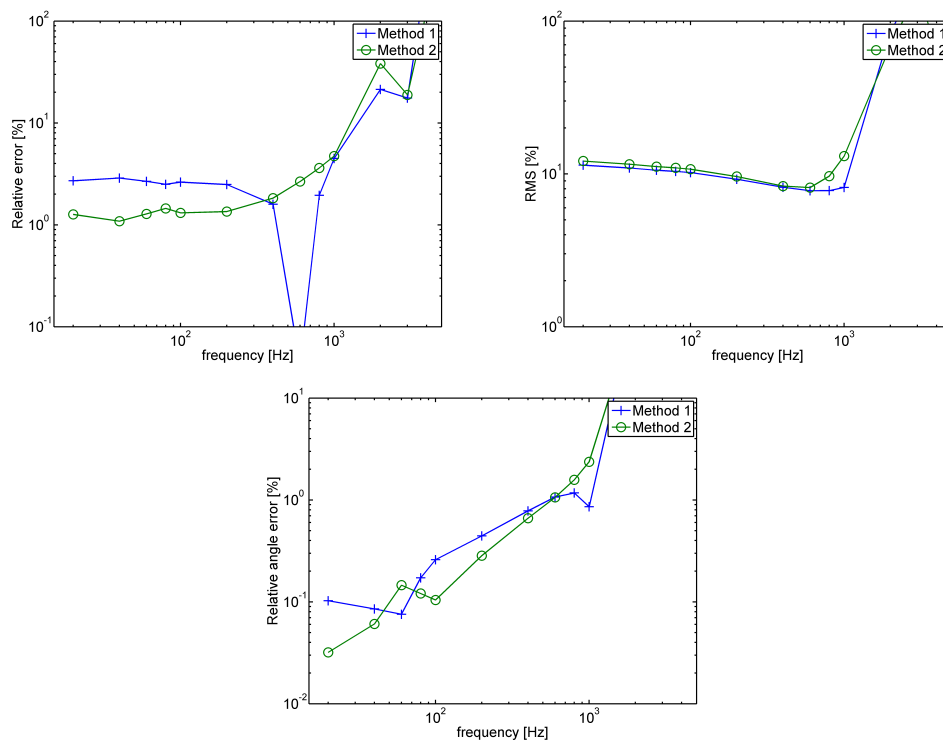


Figure 4.2.5: Errors versus the frequency of the source

#### 4.2.4 Size of the holograms

Earlier simulations resulted in plots like the one in figure 4.2.6.

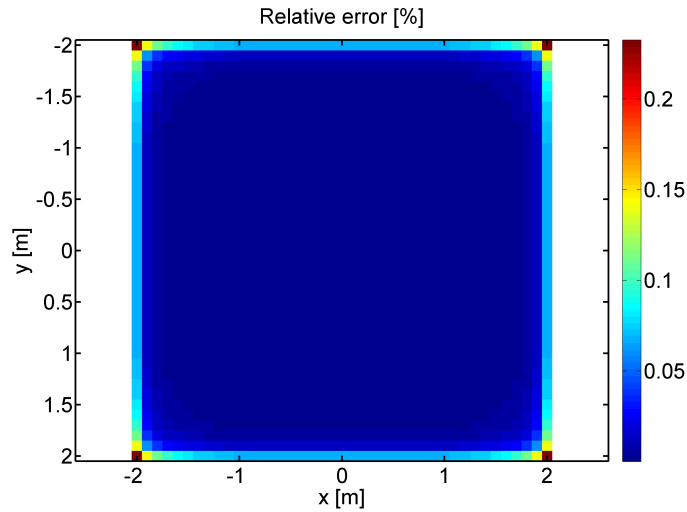


Figure 4.2.6: An example of a plot, that shows the quadratic error of every point in the plane

This plot shows the quadratic errors and it usually showed that the center point of the plane gave the most accurate results. And, while checking the plane from the center to the side, it showed that the error kept increasing. This effect is probably caused by a combination of two things. First there is the fact that the cosine in the propagation equation, creates the effect that the information of the plane at  $z = z_s$  directly below a point of the hologram plane is much more important than the information which is not directly below that point. This is shown in figure 4.2.7a.

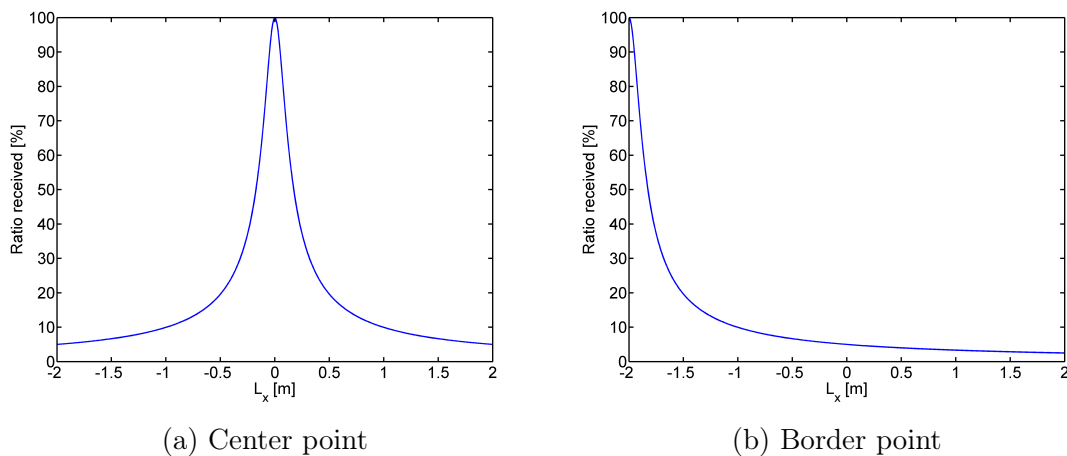


Figure 4.2.7: Influence of cosine

This means that the center point of the hologram plane gets lots of information of the plane below and probably does not even notice that the wave field at  $z = z_s$  is finite. While a point positioned further at the side only gets a part of the information it actually needs for a correct propagation, shown in figure 4.2.7b. This effect will now be analysed by first increasing the size of both planes. Secondly only the size of plane at  $z = z_s$  is increased. In both cases the center point receives the same information so it should give similar results, while points at the side will receive more information when only plane at  $z = z_s$  is increased. Results of increasing the size of both planes are shown in 4.2.8 and results of increasing the size of only the plane at  $z = z_s$  are shown in figure 4.2.9. The relative error and relative angle error do indeed show that the center point's error is constant in both cases. When now the RMS errors are compared it does clearly show that on average the error becomes much lower when only the plane at  $z = z_s$  is increased, resulting in more information for the sides of the plane and thus a more accurate result. It also shows that the RMS error decreases when both plane sizes are increased. This is caused by the fact that now more points, which receive on average more information, are present in the plane.

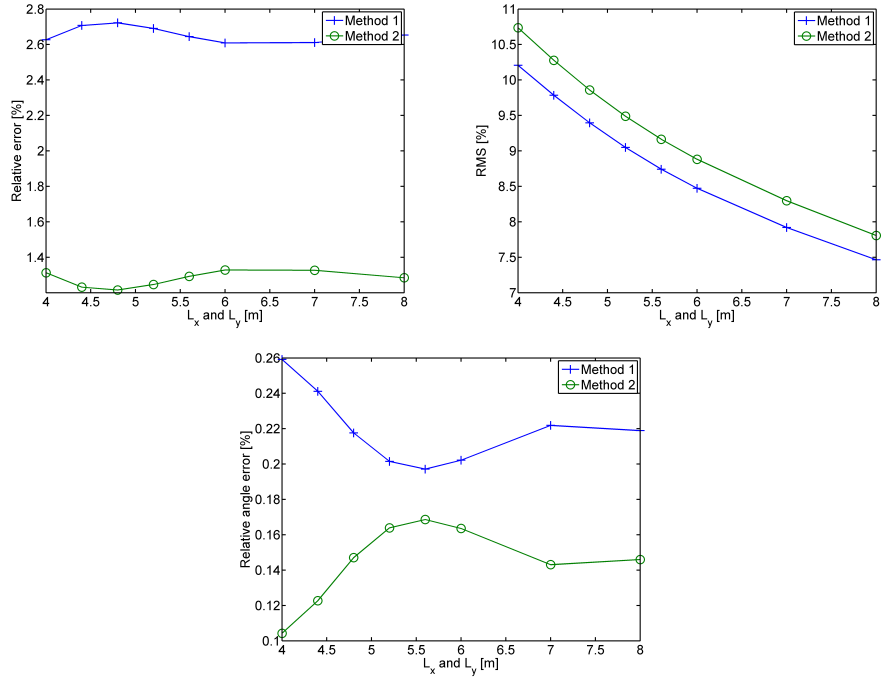


Figure 4.2.8: Errors versus the increase of the size of both planes

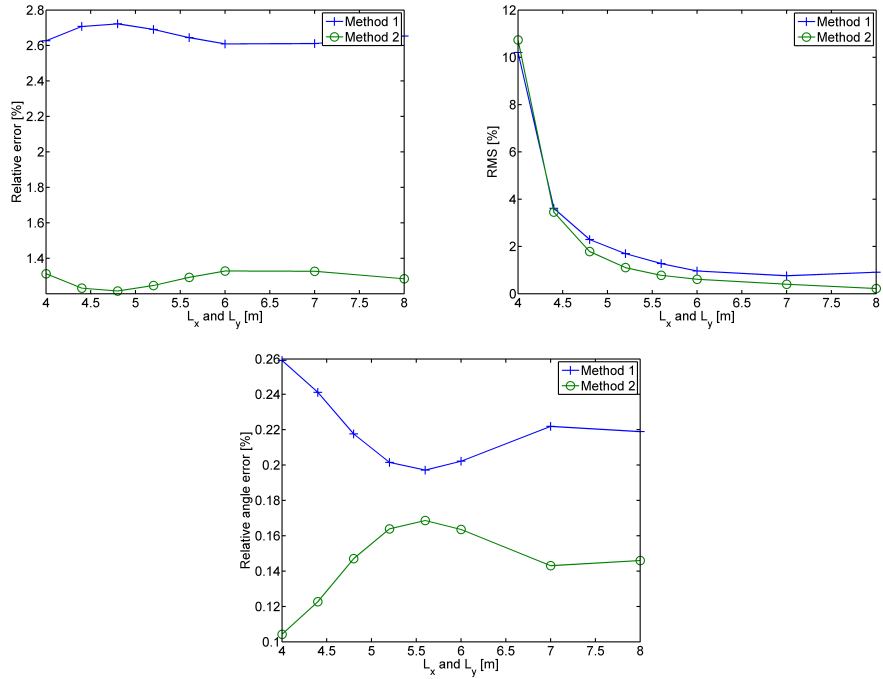


Figure 4.2.9: Errors versus the increase of only the size of the plane at  $p_{z_s}$

## 4.2.5 Resolution of the wave field

Finally the effect of the resolution,  $\Delta x$  and  $\Delta y$ , of the wave field is examined for method 1. It is expected that increasing the resolution will result in a higher accuracy of method 1, especially when the distance between the planes becomes smaller.

These results are shown in figure 4.2.10. This shows that the error does decrease for a higher resolution. The relative error of the center point does even give better results than method 2. This can be explained by the fact that increasing the resolution also means that the plane contains much more information of the wave field. But it also shows that when the distance between the planes is small, method 1 can't give an accurate propagation and can't compete against the integral of method 2. There is only a striking point in the relative angle error at  $z_h = 5m$ , when method 1 uses a resolution of  $0.5m$ , it give a very low error. The other graphs do not show this behaviour. It gives the same sort of result earlier noticed in the relative error of the frequency simulation, of which no clear clarification is determined.

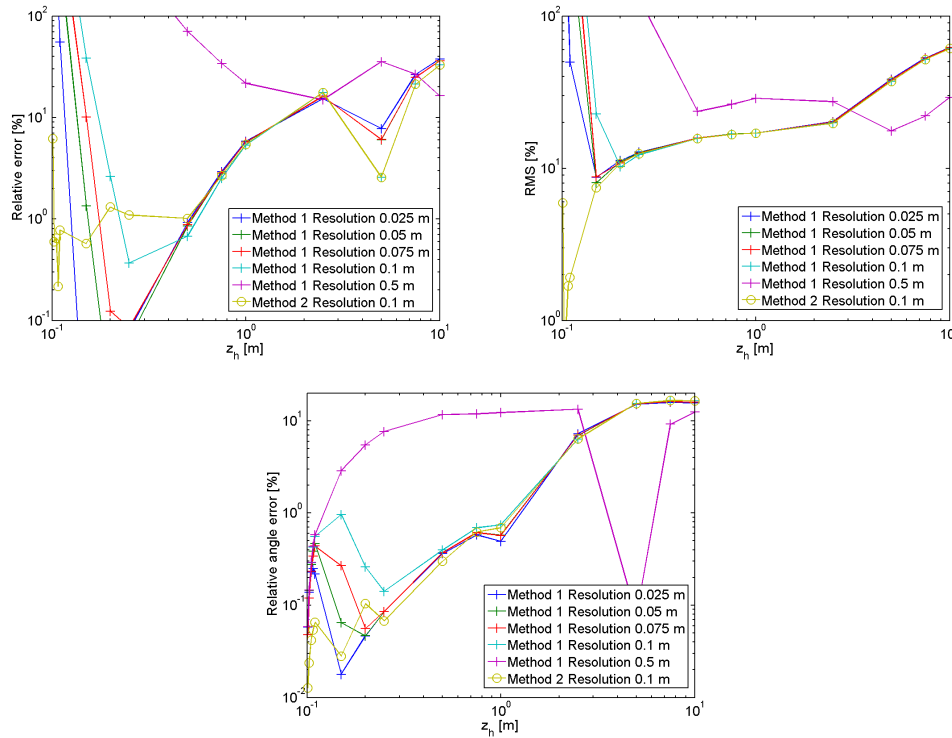


Figure 4.2.10: Errors versus the height  $z_h$  of the hologram plane, for varying the the resolution of method 1

### 4.3 Comparison between wave- and spatial-domain propagation

The spatial-domain implementation performances is now checked and the optimal wave-domain preconditioning parameters are determined. So now both implementations can be compared.

The results are shown in figure 4.3.1. These results show that, depending on the propagation distance and which information is relevant, the best approach can be chosen. When far-field propagation is needed the spatial-domain approach gives the best result judging by these graphs. For near-field propagation both approaches are sufficient when accurate information of the center point is important. The graphs show a difference between the approaches of less than one percent. When accurate information over the entire plane is required it depends again on the propagation distance. When the distance becomes lower than  $z_h = 0.2m$  spatial-domain approach gives a much more accurate result, whereas the wave-domain approach gives a more accurate result from distances higher than  $z_h = 0.2m$  in near-field.

The fact that the wavenumber-domain approach does not deliver the same results as the spatial-domain approach in the far-field propagation, can be due to the fact that for the use of the Fourier transform, preconditioning is required, which results in larger errors when the extrapolation distance becomes very large.

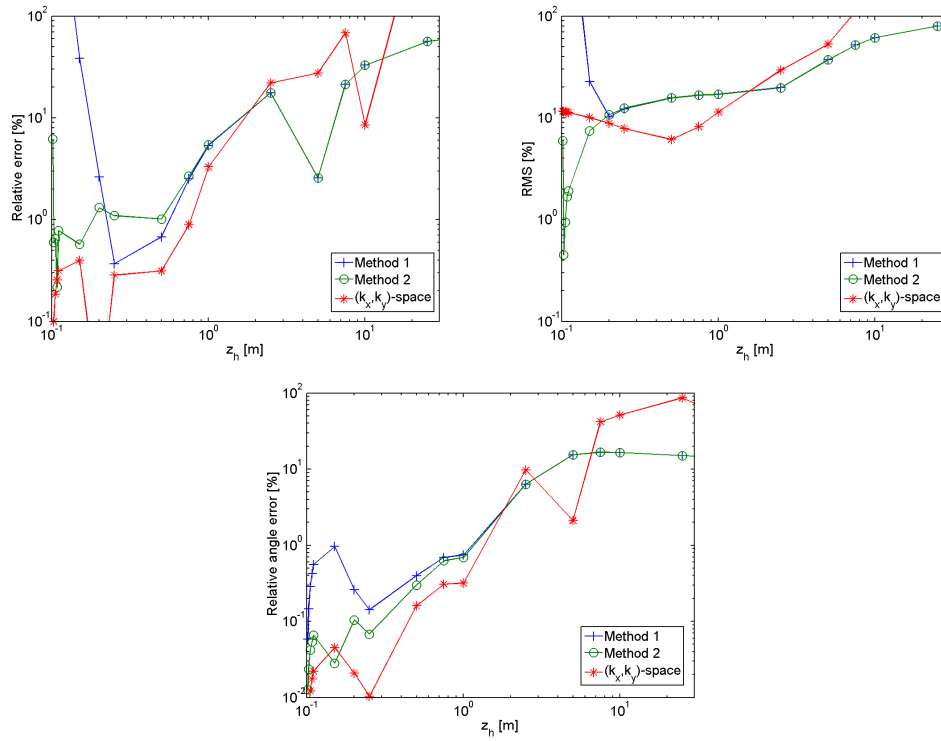


Figure 4.3.1: Errors versus the the height  $z_h$  of the hologram plane, for spatial- and wavenumber-domain implementation

# Chapter 5: Conclusion

The theory behind propagation in wavenumber-domain and in spatial domain has been studied. Using this theory a numerical implementation is finalized, which is tested and improved using simulations. After that the behaviour of the numerical implementation in spatial-domain has been discussed, which resulted in a feasible outcome. Finally the both approaches were compared.

In this study it has been tried to examine whether the spatial-domain approach, described by Berkhout [2], can achieve the same results as the approach in wavenumber-domain, described by Williams [1]. In this study this is only done for the forward propagation.

The study showed that both approaches give sufficient results for near-field forward propagation. For far-field forward propagation the spatial-domain approach gives better results. Probably caused by the fact that the wave field for wavenumber domain is adjusted, which gives a larger error when propagation over a greater distance is needed.

Recommendation for a further study are first to adjust the implementation in spatial domain so it is also able to calculate the back propagation. Also it is considered to use shape functions, which can be used to improve the performance of the implementation, by making a better approximation of the wave field using the discrete aperture points.



# Bibliography

- [1] E.G. Williams, Fourier Acoustics: Sound radiation and nearfield acoustical holography, ACADEMIC PRESS, 1999.
- [2] A.J. Berkhout, A wave field extrapolation approach to acoustical modeling in enclosed spaces, Delft University of Technology, 1998.
- [3] Danial Trad, Multiple removal based on wavefield extrapolation.
- [4] E. Skudrzyk, The Foundation of Acoustics: Basic mathematics and basic acoustics, Springer-Verlag, 1971.
- [5] J. Kok, M.J.G. van de Molengraft, Signaalanalyse, dictaat 4A250, 2006.

# Appendix A: Normal derivative of $G$

The Green function is defined as

$$G = \frac{e^{-jkr}}{r}, \quad (\text{A.1})$$

with

$$r = \sqrt{(x - x_0)^2 + (y - y_0)^2 + (z - z_0)^2}. \quad (\text{A.2})$$

The derivative can be calculated using

$$\frac{\partial G}{\partial \vec{n}} = \frac{\partial G}{\partial r} \frac{\partial r}{\partial z}. \quad (\text{A.3})$$

The derivative of  $r$  is

$$\frac{\partial r}{\partial z} = \frac{z - z_0}{r} = \cos\varphi. \quad (\text{A.4})$$

Now the derivative of  $G$  results in

$$\frac{\partial G}{\partial n} = \frac{e^{-jkr} \cdot -jk \frac{\partial r}{\partial z} \cdot r - \frac{\partial r}{\partial z} \cdot e^{-jkr}}{r^2} \quad (\text{A.5})$$

$$\frac{\partial G}{\partial n} = \frac{-e^{-jkr} jkr \cos\varphi - e^{-jkr} \cos\varphi}{r^2} \quad (\text{A.6})$$

$$\frac{\partial G}{\partial n} = -\frac{jkr + 1}{r^2} e^{-jkr} \cos\varphi \quad (\text{A.7})$$